New Insights into the Nucleolar Localization of a Plant RNA Virus-Encoded Protein That Acts in Both RNA Packaging and RNA Silencing Suppression: Involvement of Importins Alpha and…

Article *in* Molecular Plant-Microbe Interactions · May 2018

DOI: 10.1094/MPMI-02-18-0050-R

2 authors, including:

Carmen Hernández
Universitat Politècnica de València

New insights into the nucleolar localization of a plant RNA virus-encoded protein that acts in both RNA packaging and RNA silencing suppression: involvement of importins alpha and relevance for viral infection

Miryam Pérez-Cañamás, Carmen Hernández*

Instituto de Biología Molecular y Celular de Plantas (Consejo Superior de Investigaciones Científicas-Universidad Politécnica de Valencia). Ciudad Politécnica de la Innovación, Ed. 8E. Camino de Vera s/n, 46022 Valencia, Spain

* Corresponding author. Mailing address: Instituto de Biología Molecular y Celular de Plantas, (Consejo Superior de Investigaciones Científicas-Universidad Politécnica de Valencia), Ciudad Politécnica de la Innovación, Ed. 8E. Camino de Vera s/n, 46022 Valencia, Spain

Phone: 34-96-3877869 E-mail: cahernan@ibmcp.upv.es

23 **ABSTRACT**

24 **Despite replication of plus strand RNA viruses takes place in the cytoplasm of host**
25 **cells, different proteins encoded by these infectious agents have been shown to**
26 **localize in the nucleus, with high accumulation at the nucleolus. In most cases, the**
27 **molecular determinants and/or biological significance of such subcellular**
28 **localization remain elusive. Recently, we reported that protein p37 encoded by**
29 ***Pelargonium line pattern virus* (family *Tombusviridae*) acts in both RNA packaging**
30 **and RNA silencing suppression. Consistently with these functions, p37 was**
31 **detected in the cytoplasm of plant cells though it was also present in the nucleus**
32 **and, particularly, in the nucleolus. Here, we have aimed to gain further insights**
33 **into factors influencing p37 nucleolar localization and into its potential relevance**
34 **for viral infection. Besides mapping the protein region containing the nucleolar**
35 **localization signal, we have found that p37 interacts with distinct members of the**
36 **importin alpha family -main cellular transporters for nucleo-cytoplasmic traffic of**
37 **proteins-, and that these interactions are crucial for nucleolar targeting of p37.**
38 **Impairment of p37 nucleolar localization through down-regulation of importin**
39 **alpha expression resulted in a reduction of viral accumulation, suggesting that**
40 **sorting of the protein to the major subnuclear compartment is advantageous for**
41 **the infection process.**

42 **INTRODUCTION**

43

44 Viruses, as obligate intracellular parasites, must employ many cellular resources to
45 establish productive infections. Despite the replication of plus strand (+) RNA viruses
46 (either from plants or animals) occurs in the cytoplasm of host cells, distinct proteins
47 encoded by these infectious agents have been reported to enter the nucleus showing,
48 some of them, high accumulation at the nucleolus (Hiscox 2007; Salvetti and Greco
49 2014; Taliansky et al. 2010). In most cases, the biological meaning of such subcellular
50 localization remains obscure. Moreover, information on the structural determinants
51 and/or host factors that are involved in the nuclear/nucleolar targeting of the
52 corresponding protein is frequently scarce.

53 Current knowledge indicates that nucleo-cytoplasmatic trafficking of most proteins is
54 an active process that takes place through the nuclear pore complex (NPC) and usually
55 follows the classical import pathway. In this pathway, proteins destined for transport to
56 the nucleus contain a so-called nuclear localization signal (NLS) within their primary
57 sequence that is recognized by heterodimeric nuclear-cytoplasmic shuttling receptor
58 consisting of importin alpha and importin beta. Importin alpha component plays a
59 central role as adaptor molecule mediating interaction between the cargo and importin
60 beta which, in turn, facilitates passage of the cargo-importin alpha transient complex
61 through the central transporter of NPC (MacPherson et al. 2015). Once inside the
62 nucleus, some proteins remain in the nucleoplasm whereas others associate to
63 subnuclear bodies being the nucleolus the most prominent one with a typical size that
64 can reach up to 8 μm. Nucleolus has a well-known role in rRNA transcription,
65 processing and ribosome biogenesis but in the last years it has been involved in a
66 growing number of additional functions including cell cycle regulation, gene silencing,

67 senescence, stress responses, and biogenesis of multiple kinds of ribonucleoprotein
68 (RNP) particles (Boisvert et al. 2007; Olson and Dundr 2015; Shaw 2015). The
69 localization of proteins to the nucleolus has not been shown to involve active transport
70 mechanisms and is typically dictated by interaction with nucleolar core components, yet
71 in most of the cases depends on the presence of nucleolar localization signal(s) (NoLSs)
72 (Carmo-Fonseca et al. 2000; Emmott and Hiscox, 2009; Martin et al. 2015).

73 *Pelargonium line pattern virus* (PLPV) is a (+) RNA virus which belongs to a new
74 genus –*Pelarspovirus*- within the broad family *Tombusviridae* (Castaño and Hernández
75 2005; Castaño et al. 2009; Scheets et al. 2015). Its monopartite genome encodes five
76 proteins, one of which, with a molecular weight of 37 kDa (p37), has been reported to
77 act as both coat protein (CP) and viral RNA silencing suppressor (VSR) (Pérez-
78 Cañamás and Hernández 2015). Analysis of the subcellular distribution of a green
79 fluorescent protein (GFP)-tagged p37 transiently expressed in *Nicotiana benthamiana*
80 leaves showed that p37 localizes in the cytoplasm of plant cells (Pérez-Cañamás and
81 Hernández 2015). However, though no NLS (nor NoLS) could be predicted in the
82 protein by *in silico* approaches, GFP-tagged p37 was also found inside the nucleus, with
83 preponderant accumulation at the nucleolus. The biological implications of the
84 nuclear/nucleolar targeting of p37 are so far uncertain as, apparently, it does not
85 significantly influence either of the two identified functions of the protein,
86 encapsidation and RNA silencing suppression (Pérez-Cañamás and Hernández 2015).
87 Such targeting could thus be related with unknown roles of the protein during the
88 infection process or, alternatively, with some host defence mechanism aimed to reduce
89 VSR impact on host endogenous pathways and/or to restrict viral infection by
90 precluding encapsidation and antiviral silencing inhibition. Indeed, recent results

91 suggest that the VSR activity of PLPV must be tightly regulated during infection as the
92 virus is a very efficient target of RNA silencing (Pérez-Cañamás et al. 2017).

93 Here we have intended to get further insights into the molecular determinants for
94 nuclear/nucleolar localization of PLPV p37. Firstly, we have studied the subcellular
95 distribution of untagged p37 in the context of a real viral infection. Secondly, we have
96 attempted to delimit the boundaries of the structural motif directing p37 to nucleolus.
97 Thirdly, we have explored, through bimolecular fluorescence complementation (BiFC)
98 and RNA interference (RNAi) assays, the potential involvement of importins alpha in
99 nuclear/nucleolar targeting of p37. As such participation has been confirmed, we have
100 tackled whether down-regulation of importins alpha, leading to impairment of the
101 nuclear/nucleolar targeting of p37, has any effect on virus accumulation. On the basis of
102 the obtained results, presumptive roles of the subcellular partitioning of PLPV p37 are
103 further discussed.

104

105 **RESULTS**

106

107 **PLPV p37 produced during viral infection shows cytoplasmic and nuclear/**
108 **nucleolar distribution paralleling that found for transiently expressed GFP-tagged**
109 **p37.**

110 The pattern of subcellular distribution of a protein may be affected by multiple
111 factors and can undergo substantial alterations in response to environmental conditions
112 (Görner et al. 1998; Henke et al. 2011; Noirot et al. 2014). Moreover, incorporation of a
113 tag into a protein may have a significant impact in protein´s actual behavior (Bouia et al.
114 2001; Brothers et al. 2003; Ledent et al. 1997). As mentioned above, previous work
115 showed that transiently expressed GFP-tagged p37 localized in the cytoplasm and the
116 nucleus/nucleolus of plant cells (Pérez-Cañamás and Hernández 2015). We wondered

117 whether this intracellular distribution could be extrapolated seamlessly to the unfused
118 protein and, moreover, to that produced in the course of a real infection. To answer this
119 question, systemic leaves from PLPV-infected *N. benthamina* plants were used as
120 starting material to obtain cytoplasm- and nuclei-enriched fractions. For comparison
121 purposes, *N. benthamiana* leaves were agroinfiltrated with constructs for transient
122 expression of GFP-tagged or untagged p37, and, three days after infiltration (d.p.if.),
123 this plant material was used to prepare the same type of fractions. Western blot analysis
124 of the obtained samples using an antibody against UDP-glucose pyrophosphorylase
125 (UDP, cytoplasmic marker) and Histone 3 (H3, nuclear marker) supported the reliability
126 of the fractionation since the former protein was detectable in the cytoplasmic fractions
127 but undetectable in the nuclear ones and the opposite was found for the latter (Fig. 1).
128 Analysis of samples prepared from leaves expressing GFP-tagged p37 with a p37-
129 specific antibody revealed the presence of the fusion protein in both the cytoplasmic and
130 the nuclear fractions (Fig. 1, left panel), in agreement with the results of confocal
131 microscopy examinations (Pérez-Cañamás and Hernández 2015). Similarly, untagged
132 p37 expressed either transiently through agroinfiltration or during viral infection was
133 distributed between cytoplasmic and nuclear fractions (Fig. 1, central and right panels).
134 These observations further substantiated previous results on the subcellular localization
135 of the p37 and indicated that neither the tag nor the context of viral infection has a
136 significant impact on the distribution of the protein within the cell.
137

138 **Nucleolar targeting of p37 is directed by a short stretch of N-terminal amino acid**
139 **residues.**

140 Though programs for subcellular localization prediction did not recognize any NoLS
141 (nor NLS) in the p37 molecule, previous mutational analysis suggested that non-

142 conventional NoLS(s) must be present at the N-terminus of the protein and identified
143 several amino acid residues (aa) relevant for the nucleolar localization. Specifically,
144 alanine replacement of either two arginines at positions 15 and 16, respectively, or of a
145 tryptophan at position 28 in the GFP-tagged p37, abolished nucleolar localization of the
146 fusion protein (Pérez-Cañamás and Hernández 2015) (Fig. 2A). In order to corroborate
147 the involvement of the N-terminal region of p37 in nucleolar targeting and to discard
148 the contribution of other protein segments to localization in such subnuclear
149 compartment, the N-terminal (aa 1-77), middle (aa 78-232) and C-terminal (aa 233-338)
150 domains of p37 were separately fused in frame to GFP. The resulting recombinant
151 proteins were transiently expressed, along with monomeric red fluorescent protein
152 (mRFP)-tagged fibrillarin (used as nucleolar marker; Kim et al. 2007), in *N.*
153 *benthamiana* leaves via agroinfiltration. Assessment of the subcellular distribution of
154 the GFP-tagged proteins through confocal microscopy showed that only that embracing
155 the N-terminal domain retained the nucleolar localization ($p37_{1-77}$:GFP in Fig. 2),
156 confirming that this domain contains the signal(s) that direct p37 to nucleoli. To further
157 delimit the p37 region that is required for nucleolar targeting, various deletions were
158 introduced into the N-terminal domain to create a new series of GFP fusion proteins.
159 These proteins included, respectively, aa 1-60, 1-45, 1-32 and 13-45 of the p37
160 molecule (Fig. 2). Inspection of the subcellular distribution of the engineered proteins
161 showed that the stretch harbouring the most N-terminal 45 aa was sufficient for
162 nucleolar localization ($p37_{1-45}$:GFP in Fig. 2B). Additional deletions of N-terminal
163 ($p37_{13-45}$:GFP) or C-terminal ($p37_{1-32}$:GFP) amino acids led to nucleolar exclusion (Fig.
164 2B). Collectively, the results allowed us to delimit the NoLS-containing region of p37
165 to the first N-terminal 45 aa which, moreover, was consistent with previous outcomes
166 with p37 mutants (Pérez-Cañamás and Hernández 2015).

167

168 **PLPV p37 interacts with distinct importins alpha.**

169 As indicated above, nucleo-cytoplasmatic trafficking of proteins takes place through
170 the NPC and usually follows the classical import pathway in which members of
171 importin alpha family play a central role. In *N. benthamiana*, this family is composed by
172 fourteen members that can be grouped in three major phylogenetic clusters (I, II and
173 III), the first of which can be further subdivided into three subclusters (Ia, Ib, Ic) (Fig.
174 3A). In order to assess whether p37 importins alpha are able to recognize p37 to mediate
175 its transport to the nucleus and, in turn, the nucleolus, we explored, through BiFC
176 assays, potential interactions between p37 and representatives of the distinct
177 clusters/subclusters of importin alpha family. To this end, constructs for transient
178 expression of five different importins alpha (belonging to subclusters Ia, Ib and Ic, and
179 clusters II and III, respectively) fused to the N- or C-terminal part of the superyellow
180 fluorescent protein (sYFP) were generated. These constructs were used in proper
181 combinations with others allowing transient expression of p37 fused to the N- or C-
182 terminal part of sYFP (Pérez-Cañamás and Hernández 2015). *N. benthamiana* cells co-
183 expressing sYFPN-p37 and any of the sYFPC-importin alpha members showed clear
184 sYFP-derived fluorescence indicating reconstitution of the fluorophore and, thus,
185 demonstrating that p37 is able to interact with members of the importin alpha family
186 included into distinct clusters/subclusters (Fig. 3B). Similar results were obtained with
187 reverse protein combinations, i.e., when sYFPC-p37 was co-expressed with any of the
188 sYFPN-importin alpha fusion proteins (data not shown). Moreover, control experiments
189 in which the distinct fusion proteins were co-expressed with unfused sYFP halves
190 (example in row F of Fig. 3B) did not result in any significant fluorescence, reinforcing
191 the validity of detected interactions. Interestingly, in most cases the fluorescence was

192 essentially localized in the nucleus and particularly concentrated at the nucleolus
193 suggesting that the interaction between the two partners, p37 and importin alpha of any
194 type, mostly occurs and/or is maintained in this subnuclear body. The only exception
195 corresponded to the importin alpha representative of clade III for which the interaction
196 with p37 was detected not only in the nucleus and nucleolus, but also in the cytoplasm
197 (row E in Fig. 3B). In addition, the latter interaction was apparently weaker than that
198 observed with the remaining importins alpha included in the study, though reconstituted
199 fluorescence was clear when compared with the results of negative controls (images of
200 row E *versus* that of row F in Fig. 3B).

201 Besides the BiFC approach, a co-immunoprecipitation assay was performed to
202 further corroborate the interaction of p37 with importin alpha of clade III. To this aim,
203 the importin alpha representative of clade III and also that of subclade Ia, used as
204 positive control, were fused in frame to an histidine (His) tag and transiently expressed
205 in *N. benthamiana* leaves along with p37. After protein extraction, immunoprecipitates
206 were obtained using an antibody against the His tag. Western blot analysis with the anti-
207 His antibody revealed the presence of importins alpha of clade III and subclade Ia in the
208 corresponding immunoprecipitates, as expected (Fig. 3C, upper panels). Remarkably,
209 p37 was also present in those immunoprecipitates, confirming the interaction between
210 both types of proteins as showed by the BiFC assays (Fig. 3C, lower panels). No p37
211 was detected when neither importin alpha was included in the input extracts supporting
212 the reliability of the immunoprecipitation procedure (Fig. 3C). Collectively, the results
213 of this section indicated, on one side, that p37 is able to interact with members of all
214 groups of importin alpha family, and, on the other, that such interaction takes place
215 mainly at the nucleus and, especially, at the nucleolus. It is worth mentioning that
216 mRFP-tagged importin alpha proteins, at least those corresponding to the representative

217 members of subclades Ia and Ib (also annotated as importin alpha 1 and 2, respectively;
218 Fig. 3), have been shown to have a nuclear localization with high accumulation at the
219 nucleolus (Kanneganti et al. 2007) and, thus, the distribution pattern of the interaction
220 of p37 with importins alpha reproduces that of the latter ones.
221
222 **Down-regulation of importins-alpha through RNAi severely impairs nucleolar**
223 **localization of p37.**
224 In the light of the results from BiFC assays, we wondered whether importins alpha
225 could be one of the key host factors determining localization of p37 at the nucleolus. To
226 answer this question, we down-regulated the expression levels of importins alpha using
227 an RNAi approach. More specifically, we designed five binary constructs with
228 expression cassettes that, after delivery via agroinfiltration into plant leaves, would
229 yield hairpin transcripts able to impair expression of importins alpha included in
230 clades/subclades II, III, Ia, Ib and Ic, respectively, through RNA silencing. The gene
231 segments for RNAi constructs of each importin alpha clade/subclade were carefully
232 selected from specific gene regions to reasonably ensure silencing of members
233 belonging to a given phylogenetic group/subgroup and not to other groups/subgroups.
234 *N. benthamiana* leaves co-infiltrated with a mixture of *Agrobacterium tumefaciens*
235 strains transformed with each of these constructs showed reduced accumulation of the
236 distinct importin alpha members as it could be corroborated by semi-quantitative
237 reverse transcription (RT)-PCR assays (Fig. 4A). When the RNAi constructs were
238 assayed separately, reduction in expression levels induced by each RNAi construct was
239 found to be clade-specific, as desired, though some cross-target silencing was observed
240 for members of subclades within clade I (e.g. Fig 4B), most likely dictated by their high
241 sequence conservation. Despite such cross-reaction, employment of all three subclade
242 constructs was considered useful in the following assays, on one side, because they

243 could reinforce silencing of importins alpha of clade I when combined and, on the other,
244 because they could provide results that should be comparable each other when used
245 individually.

246 Analysis of the subcellular distribution of transiently expressed GFP-tagged p37 in
247 plant cells with reduced expression of importins alpha of the different clades/subclades
248 showed substantial loss of nucleolar localization (Fig. 4C). Nucleolar localization of
249 p37 reached percentages as low as 28 % when all importins alpha were simultaneously
250 silenced, which contrasted with the total lack of p37 nucleolar exclusion in leaves
251 agroinfiltrated with an empty RNAi vector used as negative control for importin alpha
252 silencing (Fig. 4C). Underlining the specificity of the assay, nucleolar localization of
253 mRFP-tagged fibrillarin was not affected by importin alpha depletion (Fig. 4C and data
254 not shown), in agreement with previous results showing that targeting of fibrillarin to
255 the nucleus/nucleolus was independent of, at least, importins alpha 1 and 2 (Kanneganti
256 et al. 2007). Collectively, the results strongly supported that importins alpha play an
257 essential role in the nucleolar targeting of p37.

258

259 **Impairment of importin alpha expression correlates with decreased accumulation**
260 **of PLPV at early stages of infection.**

261 As shown above, depletion of importins alpha negatively affected the
262 nuclear/nucleolar localization of p37. To assess whether such depletion had also an
263 impact on the progress of viral infection, the RNAi approach was once more employed
264 to silence importins alpha. The importin alpha-silenced leaves, along with mock
265 agroinfiltrated controls, were inoculated with PLPV. Leaves were collected at 1, 2, 3,
266 and 7 days post-inoculation (d.p.i.) and subjected to Northern blot analysis to check
267 PLPV accumulation. The results showed a notable decrease in viral titers in the

268 importin alpha-silenced leaves with regard the non-silenced controls at early times of
269 infection (compare signal intensities in lanes b and c with those of lanes f and g,
270 respectively, in Fig. 5A). Such decrease was no longer evident at 7 d.p.i., a time point in
271 which the virus had apparently reached saturating levels in either sample (lanes d and h
272 in Fig. 5A). Quantitative RT-PCR (RT-qPCR) performed on samples collected at two
273 time points, 3 and 7 d.p.i,, corroborated, on one side, the efficient importin alpha
274 silencing driven by the RNAi approach (Fig. 5B, right panel), and, on the other, the
275 significant reduction of PLPV accumulation in importin alpha-silenced *versus* non-
276 silenced leaves at 3 d.p.i. (Fig. 5B, left panel). As could be inferred by the Northern blot
277 analysis, RT-qPCR data indicated that differences in viral accumulation were not
278 significant at 7 d.p.i., suggesting that the virus overcomes the detrimental effect caused
279 by importin alpha down-regulation at later stages of infection (Fig. 5). We tried to
280 complement the results of the RNAi approach through a *Tobacco rattle virus* (TRV)-
281 based virus induced gene silencing (VIGS) assay (Bachan and Dinesh-Kumar 2012).
282 However, TRV infection of *N. benthamiana* plants initiated with a TRV vector either
283 empty or with importin alpha gene fragments, precluded subsequent PLPV infection in
284 local and/or systemic leaves (data not shown) suggesting that TRV multiplication
285 outcompetes that of PLPV. Though this prevented us from using a VIGS assay to
286 assess the potential relevance of importins alpha in the biological cycle of PLPV, the
287 results of the RNAi approach were clear and showed that impairment of importin alpha
288 expression adversely affects PLPV accumulation. As such impairment hampered
289 nucleolar localization of p37 (Fig. 4), a correlation between the loss of p37 nucleolar
290 targeting and a decrease in PLPV titers could be established.
291
292

293 **DISCUSSION**

294

295 In this work, we have obtained new and relevant insights into determinants for
296 nucleolar localization of PLPV p37, a viral protein with a dual role as CP and VSR. In
297 the first place, we have delimited the NoLS-containing region to the most N-terminal 45
298 amino acid residues. Systematic analysis of confirmed NoLSs has revealed a great
299 sequence diversity which makes NolSs particularly difficult to predict. Despite such
300 difficulty, some common traits can be noticed that are also shared by the p37 NoLS
301 including an N-terminal location and a considerable enrichment in basic amino acids
302 (Fig. 2) (Martin et al. 2015; Scott et al. 2010). As stated previously (Pérez-Cañamás and
303 Hernández 2015), the NoLS-containing region of p37 is also involved in other relevant
304 properties of the protein such as the capacity to bind small RNAs, which is essential for
305 its VSR function. In addition, it forms very likely part of the so-called RNA binding
306 domain that has been proposed to directly interact with viral ssRNA for virion
307 formation in related CPs (Sit and Lommel 2015; Rao et al. 2006). These observations
308 emphasize once more the high overlap of motifs involved in different functional traits of
309 p37, as we stressed in a previous study (Pérez-Cañamás and Hernández 2015).

310 Besides delineating the NoLS-containing region, we have obtained results supporting
311 that subcellular localization of p37 is not affected either by its fusion to a tag or, more
312 importantly, in the context of a real infection. This is not a trivial issue as cellular
313 compartmentalization of a protein –either viral or cellular- may undergo relevant
314 alterations during cell cycle or under different environmental conditions, all the more is
315 this the case when an active process of viral infection is ongoing (Drissi et al. 2013;
316 Alexander and Cilia 2016). The presence of other PLPV proteins besides p37, the
317 complex network of interactions that can be established between them and host proteins

318 and the profound effects that a replicating virus may have on host cellular functions
319 might have resulted in significant discrepancies in the subcelullar localization of a
320 transiently expressed GFP-tagged protein and that produced during a genuine viral
321 infection process, and our results have ruled out that possibility.

322 We have also shown that p37 is able to interact with different members of the
323 importin alpha family and, moreover, that such interaction most likely dictates the
324 nucleolar localization of the viral product. These observations suggest that the protein
325 has evolved the mechanisms to ensure its nuclear/nucleolar import regardless changes in
326 the level of a specific type of importin alpha. Such redundancy in the nuclear traffic of
327 viral proteins is not unusual and has been reported previously for proteins encoded by
328 animal, fungi as well as plant viruses such as the TGB1 of a pomovirus whose
329 nuclear/nuclear localization was affected by knockdown of two distinct importins alpha
330 (Kanneganti et al. 2007; König et al. 2010; Lukhovitskaya et al. 2015; Melen et al.
331 2003; O'Neill et al. 1995; Smith et al. 1997). In addition, we cannot completely discard
332 the involvement of other nuclear import pathways, besides the classical importin
333 alpha/importin beta pathway, in the nuclear/nucleolar targeting of p37. Indeed, though
334 the presence of the protein in the nucleolus was strongly reduced by down-regulation of
335 importins alpha, a non-negligible amount of the protein was still evident in the
336 nucleoplasm of cells that showed nucleolar exclusion of p37 (Fig. 4B), suggesting that
337 mechanisms distinct from those involving importin alpha may contribute somehow to
338 the nuclear sorting of p37.

339 The ultimate reasons of the nucleolar (and/or nuclear) targeting of p37 remains
340 elusive as occurs with other proteins that show this subcellular localization. Previous
341 work showed that it was not strictly required for either the encapsidation or the VSR
342 function of PLPV p37 (Pérez-Cañamás and Hernández 2015) but here we have shown

343 that impairment of such localization through importin alpha knowdown negatively
344 affects viral accumulation. Several scenarios can be envisioned to explain these
345 observations. Firstly, it is possible that importin alpha-mediated transport of p37, the
346 most abundantly produced viral protein during PLPV infection, significantly interferes
347 with the conventional pathway for cytoplasmic-nuclear shuttling of host proteins, thus
348 changing cellular homeostasis to favor the infectious process. Alternatively, p37
349 confinement in the nucleolus might help to regulate viral protein ratios, an essential
350 issue for virus survival (Castaño et al. 2009). This compartmentalization based-
351 regulation could rely just on the removal of part of p37 molecules from the cytoplasm to
352 maintain the required protein amounts in this cellular compartment -where PLPV
353 replication cycle takes place-, with the nucleolus functioning as a kind of p37 garbage
354 disposal or even more actively contributing to p37 turnover. With regard to the latter, it
355 is interesting to mention that a proteosome-independent pathway for protein degradation
356 has been reported in the nucleolus of animal cells (Tao et al. 2013), and the existence of
357 a similar pathway in plant cells cannot be completely ruled out. Finally, the presence of
358 p37 in the nucleolus could be related with an unknown function of the protein aimed to
359 manipulate host nucleolar processes for virus own benefit such as, for instance, RNA
360 silencing or ribosome biogenesis. The recruitment of some nucleolar component(s) by
361 p37 that might be essential for PLPV biological cycle can neither be excluded. In this
362 connection, one of the few plant viral proteins for which a biological significance of its
363 nucleolar localization has been advanced is that encoded by the ORF3 of an umbravirus
364 (*Groundnut rosette virus*), a type of plant RNA virus that does not produce a CP and
365 that also belongs to family *Tombusviridae*. The umbravirus ORF3-encoded product is
366 involved in virus long-distance movement and has been proposed to hijack and
367 relocalize fibrillarin from the nucleolus to the cytoplasm to participate in formation of

368 viral RNPs. These RNPs protect viral RNAs and move through the floem, determining
369 the ability of umbravirus to cause systemic infection (Kim et al. 2007). Interactions of
370 some additional plant virus proteins (or RNAs) with fibrillarin and/or with other
371 nucleolar components have been reported though their precise role during viral
372 infectious cycle is mostly unclear (Jiang et al. 2009; Rajamäki et al. 2009; Semashko et
373 al. 2012; Shaw et al. 2014; Zheng et al. 2015). More investigation is being carried out in
374 an attempt to gain further insights into the precise biological meaning of the nucleolar
375 localization of PLPV p37.
376

377 **MATERIALS AND METHODS**

378

379 **Plant material.**

380 *N. benthamiana* plants were grown from seeds in the greenhouse, under a 16 h
381 photoperiod and temperatures of 24 ºC and 20 ºC during day and night, respectively.
382

383 **DNA constructs.**

384 For PLPV inoculation, a pMOG800-based binary construct containing an infectious
385 cDNA flanked by the *Cauliflower mosaic virus* (CaMV) 35S promoter and the
386 terminator sequence of the *Solanum tuberosum* proteinase inhibitor II gene (PoPit), was
387 used (Castaño et al. 2009).

388 For protein subcellular localization assays, a pMOG800-based binary construct
389 containing an expression cassette with the p37 gene either unfused or fused in frame to
390 the 5´ end of the GFP gene and flanked by the CaMV 35S promoter and the PoPit, has
391 been described previously (Pérez-Cañamás and Hernández 2015). Selected regions of
392 the p37 gene were PCR amplified with KAPA HiFi DNA polymerase (Kapa

393 Biosystems) and suitable oligonucleotide primers to generate, following standard
394 cloning procedures, similar pMOG800-based constructs for expression of truncated
395 versions of p37 fused to the GFP. Binary constructs for expression of fibrillarin fused to
396 mRFP (used as nucleolar marker) or of the tombusvirus p19 (used for VSR function in
397 some experiments), have been described somewhere else (Kim et al. 2007; Martínez-
398 Turiño and Hernández 2009).

399 For BiFC assays, pROK2-sYFPN and pROK2-sYFPC-based plasmids directing
400 expression of the p37 fused to the N- and C-terminal halves of the sYFP (aa 1 to 154
401 and 155 to 238, respectively) have been reported previously (Pérez-Cañamás and
402 Hernández 2015). Similar pROK2-based constructs were generated for representative
403 members of the importin alpha family. Specifically, sequences from the five importins
404 alpha depicted in colours in Fig. 3A (representative of subclades Ia, Ib, and Ic and
405 clades II and III, respectively) were retrieved from the Sol Genomics Network database
406 (http://solgenomics.net/) to design specific oligonucleotide primers that were used to
407 amplify the corresponding full-length genes through RT-PCR using SuperScript III
408 One-Step RT-PCR System (Thermo Fisher Scientific) and total RNA extracts from *N.*
409 *benthamiana* as templates. The primers included appropriate restriction sites to facilitate
410 cloning of the amplified cDNA into pROK2-sYFPN and pROK2-sYFPC plasmids.

411 For co-immunoprecipitation assays, the importins alpha representatives of subclade
412 Ia and clade III were PCR amplified from the corresponding BiFC constructs using
413 KAPA HiFi PCR kit (Kapa Biosystems) and specific oligonucleotide primers derived
414 from the 5´ and 3´ gene termini. The reverse primers contained 5´-extra nucleotides
415 encoding six His in order to fuse a His tag to the C-terminus of the gene products. In
416 addition, forward and reverse primers harboured proper restriction sites to help cloning

417 of the amplified genes into pMOG800 vector under the control of CaMV 35S promoter
418 and PoPit terminator.

419 For RNAi assays, cDNA fragments were RT-PCR amplified from conserved regions
420 of the importin alpha genes belonging to each phylogenetic clade/subclade (Ia, Ib, Ic, II
421 and III). Five cDNAs were generated using specific oligonucleotides bearing proper
422 restriction sites at their 5´-end which expedited their insertion into pHANNIBAL vector
423 (Wesley et al. 2001). After digestion with the corresponding restriction enzymes, each
424 DNA fragment was inserted in sense and antisense orientation flanking, respectively,
425 the pyruvate dehydrogenase kinase intron present in pHANNIBAL vector. The resulting
426 hairpin expression cassettes, that included a CaMV 35S promoter and an *A. tumefaciens*
427 octopine synthase gene terminator, were cut out by NotI digestion and inserted into the
428 unique NotI site of binary plasmid pCLEAN-G181 (Thole et al. 2007). The empty
429 pHANNIBAL NotI cassette was also inserted into pCLEAN-G181 to produce a control
430 plasmid pChpEMPTY.

431 All constructs were routinely sequenced with an ABI PRISM DNA sequencer 377
432 (Perkin-Elmer) to corroborate the validity of the selected recombinant plasmids. The
433 primers used to generate the distinct recombinant constructs are listed in Supplementary
434 Table 1.

435

436 ***Agrobacterium*-mediated transient gene expression and virus inoculation.**

437 Binary plasmid constructs were transformed into *A. tumefaciens* strain C58C1 CH32
438 by the freeze/thaw shock method. Cultures of *A. tumefaciens* harbouring the different Ti
439 plasmids were infiltrated at an OD_{660} of 0.5 on the abaxial side of *N. benthamiana*
440 leaves (5 weeks old) using a 20 ml needleless syringe. When co-infiltrating distinct
441 bacterial cultures, equal amounts of such cultures were mixed before infiltration (final
442 OD_{660} of the mixed culture = 0.5). In the case of RNAi experiments, leaves were firstly

443 infiltrated with importin alpha hairpin constructs (individually or combined) or the
444 empty control construct and, 5 d.p.if., the same leaves were agroinfiltrated with pMOG-
445 derived construct for expression of either GFP-tagged or untagged p37 or for PLPV
446 inoculation (OD_{660}= 10^{-4}). The infiltrated plants were kept under greenhouse conditions
447 and leaf samples were taken at distinct times after infiltration.
448
449 **Confocal microcopy.**
450 In BiFC and subcellular localization assays, GFP, mRFP or reconstituted sYFP
451 fluorophores of tagged proteins were monitored in epidermal cells of *N. benthamiana*-
452 infiltrated tissue at 72 h post-infiltration using a Leica TCS SL confocal microscope
453 with an HCX PL APO ×40/1.25-0.75 oil CS objective. GFP and sYFP fluorescence was
454 recorded by excitation with 488 nm argon laser line with emission being collected
455 through band-pass filter from 505 to 550 nm. In the case of mRFP, excitation was
456 performed by means of a 543-nm green-neon laser line, and fluorescence emission was
457 collected at 610 to 630 nm.
458
459 **RNA extraction and Northern blot analysis**
460 Total RNA preparations from *N. benthamiana* leaves were obtained by phenol
461 extraction and lithium precipitation (Verwoerd et al. 1989). For Northern blot analysis,
462 4 µg total RNA was denatured by glyoxal-dimethyl sulfoxide treatment, electrophoresed
463 in 1% agarose gels and blotted to nylon membranes (Hybond N+; GE Healthcare). After
464 UV-crosslinking, membranes were incubated at 70 ºC, in the presence of 50%
465 formamide, with a ^{32}P-radioactive RNA probe for detection of PLPV RNAs. Such probe
466 was generated by *in vitro* transcription of a pBluescript KS(+)-based construct
467 containing the PLPV p37 gene (nt 2621–3637 of PLPV genome). After hybridization,

468 membranes were washed at room temperature for three times (10 min each) in 2×SSC
469 plus 0.1% SDS, and once at 55 ºC in 0.1×SSC plus 0.1% SDS.
470
471 **Semi-quantitative and RT-qPCR**
472 Total RNA preparations with a RIN (RNA integrity number, Agilent) equal to or
473 greater than 7 were treated with Turbo DNase (ThermoFisher). Assessment of down-
474 regulation of importin alpha gene expression in RNAi assays through semiquantitative
475 RT-PCR was performed as follows. One µg of treated total RNA per each sample was
476 subjected to RT-PCR amplification with SuperScript III One-Step RT-PCR System and
477 a pair of specific primers that yielded a cDNA embracing a region of the importin alpha
478 gene(s) different to that cloned into the corresponding hairpin construct(s)
479 (Supplementary Table I). The number of cycles for PCR amplification ranged from 20
480 to 30 and simultaneous amplification of an actin gene fragment was performed as
481 internal control. RT-qPCR was employed in some RNAi assays to compare viral titers
482 and to confirm silencing of importin alpha. To this aim, total RNA preparations, treated
483 as indicated above, were reverse transcribed (1 µg per reaction) with PrimeScript RT
484 reagent kit (Perfect Real Time, Takara) using either an oligo-dT primer (to generate
485 cDNAs for subsequent PCR amplification of protein phosphatase 2A- PP2A- gene,
486 employed as internal control, and importin alpha 1 gene) or, since PLPV RNAs lack a
487 poly(A) tail at the 3´end, a combination of an oligo-dT primer and a PLPV specific
488 primer (to generate cDNAs for subsequent PCR amplification of PP2A gene and of a
489 virus genome fragment, respectively). Design of primers for PCR was performed with
490 Primer-Express 2.0 software (Applied Biosystems) using the following criteria: melting
491 temperature ranging from 50ºC to 60ºC, PCR amplicon lengths of 100 to 200 bp, length
492 of primer sequences of 19 to 25 nucleotides, and guanine-cytosine content of 40% to

493 60% (Supplementary Table I). Master mix for qPCR was prepared with 5x PyroTaq
494 EvaGreen qPCR Mix Plus (ROX) (Cultek Molecular Bioline). Three biological
495 replicates (with three technical replicates each) were performed for every type of
496 sample. The PCR reactions were run and analyzed using the ABI PRISM 7700
497 Sequence detection system (Applied Biosystems Inc., Life Technologies Corp.) and
498 evaluation of the relative expression level of each gene was carried out with the relative
499 expression software tool (REST) designed by Qiagen (Hilden, Germany).
500

501 **Subcellular fractionation and Western blot analysis.**

502 Subcellular fractionation of the leaf extracts was carried out as described previously
503 for *Solanaceae* (Sikorskaite et al. 2013). Briefly, 5 g leaf material was grinded with
504 liquid nitrogen and the resulting leaf powder was thoroughly mixed with 5 volumes of
505 NIB buffer (10 mM MES-KOH -pH 5.4-, 10 mM NaCl, 10 mM KCl, 2.5 mM EDTA,
506 250 mM sucrose, 0.1 mM spermine, 0.5 mM spermidine, 1 mM DTT). The homogenate
507 was filtered through three layers of Miracloth and the recovered solution (initial extract,
508 IE) was further clarified by addition of Triton X-100 until a final concentration of 0.5 %
509 in order to accomplish lysis of contaminating organelles. After incubation for 20 min at
510 4 ºC, the homogenate was centrifuged at 1,000 x *g* for 10 min, the supernadant was
511 removed (cytoplasmic fraction, Cit) and the pellet was gently resuspended in 10 ml NIB
512 buffer. The crude preparation of nuclei was then loaded on a cushion formed by two
513 layers of 2.5 M sucrose and 60 % Percoll, respectively. Following centrifugation at
514 1,000 x *g* for 10 min, the 60 % Percoll layer, that contained most of the nuclei, was
515 collected and diluted with 5 volumes of NIB. After addition of Triton X-10 to a final
516 concentration of 0.5 %, the sample was incubated for 10 min at 4 ºC, centrifuged at
517 1,000 x *g* for 10 min and the resulting pellet was resuspended in 5 ml of NIB. The

518 nuclei preparation was then overlayed on a 35% Percoll cushion, and after
519 centrifugation at 1,000 x *g* for 10 min, the pellet was washed with NIB and finally
520 resuspended in nuclei storage buffer NBS (20% glycerol, 20 mM HEPES KOH, pH 7.2,
521 5 mM MgCl2, 1 mM DTT) (nuclear fraction, Nuc).

522 For Western blot analysis, aliquots of the obtained fractions were subjected to SDS-
523 PAGE, transferred to polyvinylidene difluoride (PVDF) membranes (Roche) and
524 immunoblotted with antisera against p37 (AS-0094, DSMZ) at 1:5,000 dilution,
525 antibody against histone 3 (AS10710, Agrisera) at 1:6,000 dilution or antibody against
526 UDP-glucose pyrophosphorylase (AS05086, Agrisera) at 1:3,000 dilution. Goat anti-
527 rabbit HRP conjugated (AS09602, Agrisera) at 1:10,000 dilution was used as secondary
528 antibody and immunoreactive bands were revealed with chemiluminescence ECL Plus
529 kit following supplier´s recommendations (GE Healthcare). Signals were recorded by
530 autoradiography and quantified with the aid of a FujiFilm LAS3000 Imager.

531

532 **Co-immunoprecipitation assays.**

533 *N. benthamiana* leaves agroinfiltrated with proper binary constructs and collected at
534 3-5 d.p.if. were ground to a fine powder with liquid nitrogen and homogenized in 4 ml/g
535 IP buffer (50 mM Tris-HCl pH 7.4, 100 mM KCl, 100 mM NaCl, 2.5 mM $MgCl_2$, 1
536 µg/ml leupeptin, 1 µg/ml aprotonin, 25 mM PMSF and one tablet of complete
537 proteinase inhibidor cocktail [Roche Life Science]). Cell debris were removed by
538 centrifugation at 12,000 x *g* for 15 min at 4 ºC twice and clarified lysates were
539 incubated with 4 µg/ml of His-probe antibody (H-3, Santa Cruz Biotechnology) for 1 h
540 at 4 ºC and then with 100 µl/ml of protein A/G agarose beads (Roche Life Science) for
541 2 h with mild rotation. Beads were recovered by centrifugation at 500 x *g* and washed
542 six times with IP buffer for 10 min at 4 ºC. Proteins were eluted of 2X protein loading

543 buffer buffer (1.25 M Tris, pH 6.8, 10% SDS, 80% glycerol, 10% β-mercaptoethanol,
544 and 0.02% bromophenol blue) after heating at 95 °C for 3 min. Western blot analysis of
545 protein inputs and immunoprecipitates for detection of p37 was performed as indicated
546 above. His-tagged importins were detected similarly using the mouse monoclonal His-
547 probe antibody H-3 at 1:5,000 dilution as primary antibody and sheep anti-mouse IgG
548 HRP conjugated (NA931, GE Healthcare) at 1:10,000 dilution as secondary antibody.
549

550 **Phylogenetic and sequence analyses.**

551 The sequences for *N. benthamiana* importin alpha proteins were retrieved from the
552 Sol Genomics Network database (http://solgenomics.net/tools/blast/index.pl). The
553 Molecular Evolutionary Genetics Analysis (MEGA7) software was used for aligning
554 sequences using the ClustalW algorithm and preparing the tree (Kumar et al., 2016).
555 Bootstrap values were calculated from 1,000 replicates of the tree. GenBank and Sol
556 Genomics Network accession numbers are indicated on the phylodendrogram.
557

558 **ACKNOWLEDGEMENTS**

559

560 We thank Cristian Mares for technical assistance and Pilar Fajardo for help in
561 generation of some constructs. This work was supported by grant BFU2015-70261 from
562 the Ministerio de Economía y Competitividad (MINECO, Spain) (to C. H). M.P.-C. was
563 the recipient of a predoctoral contract from MINECO.
564
565
566
567

568 **LITERATURE CITED**

569

570 Alexander, M. M., and Cilia, M. 2016. A molecular tug-of-war: global plant proteome
571 changes during viral infection. Current Plant Biol. 5:13-24.

572 Bachan, S., and Dinesh-Kumar, S. P. 2012. Tobacco rattle virus (TRV)-based virus-
573 induced gene silencing. Methods Mol. Biol. 894:83-92.

574 Boisvert, F.-M., van Koningsbruggen, S., Navascués, J., and Lamond, A. I. 2007. The
575 multifunctional nucleolus. Nat. Rev. Mol. Cell. Biol. 8:574-585.

576 Bouia, A., Kholti, A., Saghi, M., and Cornelis, P. 2001. In-frame fusion of a His-Cys
577 motif into the P*seudomonas aeruginosa* outer membrane OprI lipoprotein results in
578 increased metal binding capacity by *Escherichia coli*. Res. Microbiol. 152:799-804.

579 Brothers, S. P., Janovick, J. A., and Conn, P. M. 2003. Unexpected effects of epitope
580 and chimeric tags on gonadotropin-releasing hormone receptors: implications for
581 understanding the molecular etiology of hypogonadotropic hypogonadism. J. Clin.
582 Endocrinol. Metab. 88:6107-6112.

583 Carmo-Fonseca, M., Mendes-Soares, L., and Campos, I. 2000. To be or not to be in the
584 nucleolus. Nat. Cell Biol. 2: E107–112.

585 Castaño, A., and Hernández, C. 2005. Complete nucleotide sequence and genome
586 organization of *Pelargonium line pattern virus* and its relationship with the family
587 *Tombusviridae*. Arch. Virol. 150:949-965.

588 Castaño, A., Ruiz, L., and Hernández, C. 2009. Insights into the translational regulation
589 of biologically active open reading frames of *Pelargonium line pattern virus*.
590 Virology 386:417-426.

591 Drissi, R., Dubois, M. L., and Boisvert, F. M. 2013. Proteomics methods for subcellular
592 proteome analysis. FEBS J. 280:5626-5634.

593 Emmott, E., and Hiscox, J. A. 2009. Nucleolar targeting: the hub of the matter. EMBO
594 Rep. 10: 231–238.
595 Görner, W., Durchschlag, E., Martínez-Pastor, M. T., Estruch, F., Ammerer, G.,
596 Hamilton, B., Ruis, H., and Schüller C. 1998. Nuclear localization of the C2H2 zinc
597 finger protein Msn2p is regulated by stress and protein kinase A activity.Genes Dev.
598 12:586-597.
599 Henke, R. M., Dastidar, R. G., Shah, A., Cadinu, D., Yao, X., Hooda, J., and Zhang, L.
600 2011. Hypoxia elicits broad and systematic changes in protein subcellular
601 localization. Am. J. Physiol. Cell Physiol. 301:C913-928.
602 Hiscox, J. A. 2007. RNA viruses: hijacking the dynamic nucleolus. Nat. Rev.
603 Microbiol. 5:119-127.
604 Jiang, Y., Li, Z., and Nagy, P. D. 2009 Nucleolin/Nsr1p binds to the 3′ noncoding
605 region of the tombusvirus RNA and inhibits replication. Virology 2010; 396:10-20.
606 Kanneganti , T. D., Bai, X., Tsai, C. W., Win, J., Meulia, T., Goodin, M., Kamoun, S.,
607 and Hogenhout, S. A. 2007. A functional genetic assay for nuclear trafficking in
608 plants. Plant J. 50:149-158.
609 Kim, S. H., Macfarlane, S., Kalinina, N. O., Rakitina, D. V., Ryabov, E. V., Gillespie,
610 T., Haupt, S., Brown, J. W. S., and Taliansky, M. 2007. Interaction of a plant virus-
611 encoded protein with the major nucleolar protein fibrillarin is required for systemic
612 virus infection. Proc. Natl. Acad. Sci. USA 104:11115-11120.
613 König, R., Stertz, S., Zhou, Y., Inoue, A., Hoffmann, H. H., Bhattacharyya, S.,
614 Alamares, J. G., Tscherne, D. M., Ortigoza, M. B., Liang, Y., Gao, Q., Andrews, S.
615 E., Bandyopadhyay, S., De Jesus, P., Tu, B. P., Pache, L., Shih, C., Orth, A.,
616 Bonamy, G., Miraglia, L., Ideker, T., García-Sastre, A., Young, J. A., Palese, P.,

617 Shaw, M. L., and Chanda, S. K. 2010. Human host factors required for influenza
618 virus replication. Nature 463: 813–817.
619 Kumar, S., Stecher, G., and Tamura, K. 2016. MEGA7: Molecular Evolutionary
620 Genetics Analysis Version 7.0 for Bigger Datasets. Mol. Biol. Evol. 33:1870-1874.
621 Ledent, P., Duez, C., Vanhove, M., Lejeune, A., Fonzé, E., Charlier, P., Rhazi-Filali, F.,
622 Thamm, I., Guillaume, G., Samyn, B., Devreese, B., Van Beeumen, J., Lamotte-
623 Brasseur, J., and Frère, J. M. 1997. Unexpected influence of a C-terminal-fused His-
624 tag on the processing of an enzyme and on the kinetic and folding parameters. FEBS
625 Lett. 413:194-196.
626 Lukhovitskaya, N. I., Cowan, G. H., Vetukuri, R. R., Tilsner, J., Torrance, L., and
627 Savenkov, E. I. 2015. Importin-α-mediated nucleolar localization of potato mop-top
628 virus TRIPLE GENE BLOCK1 (TGB1) protein facilitates virus systemic movement,
629 whereas TGB1 self-interaction is required for cell-to-cell movement in *Nicotiana*
630 *benthamiana*. Plant Physiol. 167:738-752.
631 Martin, R. M., Ter-Avetisyan, G., Herce, H. D., Ludwig, A. K., Lättig-Tünnemann, G.,
632 and Cardoso, M. C. 2015. Principles of protein targeting to the nucleolus. Nucleus
633 6:314-325.
634 Martínez-Turiño, S., and Hernández, C. (2009) Inhibition of RNA silencing by the coat
635 protein of *Pelargonium flower break virus*: distinctions from closely related
636 suppressors. J. Gen. Virol. 90:519–525
637 McPherson, A. J., Lange, A., Doetsch, P. W., and Corbett, A. H. 2015. Nuclear–
638 cytoplasmic transport. In: eLS. John Wiley & Sons, Ltd: Chichester. DOI:
639 10.1002/9780470015902.a0001351.pub3.

640 Melen, K., Fagerlund, R., Franke, J., Kohler, M., Kinnunen, L., and Julkunen, I. 2003.
641 Importin alpha nuclear localization signal binding sites for STAT1, STAT2, and
642 influenza A virus nucleoprotein. J. Biol. Chem. 278: 28193–28200.

643 Noirot, E., Der, C., Lherminier, J., Robert, F., Moricova, P., Kiêu, K., Leborgne-Castel,
644 N., Simon-Plas, F., and Bouhidel, K. 2014. Dynamic changes in the subcellular
645 distribution of the tobacco ROS-producing enzyme RBOHD in response to the
646 oomycete elicitor cryptogein. J. Exp. Bot. 65:5011-5022.

647 Olson, M. O. J., and Dundr, M. 2015. Nucleolus: Structure and Function. In: eLS. J.
648 Wiley & sons, Ltd: Chichester. DOI: 10.1002/9780470015902.a0005975.pub3

649 O'Neill, R. E., Jaskunas, R., Blobel, G., Palese, P., and Moroianu, J. 1995. Nuclear
650 import of influenza virus RNA can be mediated by viral nucleoprotein and transport
651 factors required for protein import. J. Biol. Chem. 270:22701–22704.

652 Pérez-Cañamás, M., and Hernández, C. 2015. Key importance of small RNA binding
653 for the activity of a glycine/tryptophan (GW) motif-containing viral suppressor of
654 RNA silencing. J. Biol. Chem. 290:3106-3120.

655 Pérez-Cañamás, M., Blanco-Pérez, M., Forment, J., and Hernández, C. 2017. *Nicotiana*
656 *benthamiana* plants asymptomatically infected by *Pelargonium line pattern virus*
657 show unusually high accumulation of viral small RNAs that is neither associated
658 with DCL induction nor RDR6 activity. Virology 501:136-146.

659 Rajamäki, M. L., and Valkonen, J.P. 2009. Control of nuclear and nucleolar localization
660 of nuclear inclusion protein a of picorna-like *Potato virus* A in *Nicotiana* species.
661 Plant Cell 21:2485–2502.

662 Rao, A. L. 2006. Genome packaging by spherical plant RNA viruses. Annu. Rev.
663 Phytopathol. 44:61–87.

664 Salvetti, A., and Greco A. 2014. Viruses and the nucleolus: the fatal attraction.
665 Biochim. Biophys. Acta. 1842:840-847.

666 Semashko, M. A., González, I., Shaw, J., Leonova, O. G., Popenko, V. I., Taliansky, M.
667 E., Canto, T., and Kalinina, N. O. 2012. The extreme N-terminal domain of a
668 hordeivirusTGB1 movement protein mediates its localization to the nucleolus and
669 interaction with fibrillarin. Biochimie 94:1180-1188.

670 Shaw, P. J. 2015. Nucleolus. In: eLS. J. Wiley & sons, Ltd: Chichester. DOI:
671 10.1002/9780470015902.a0001352.pub4.

672 Shaw, J., Love, A. J., Makarova, S. S., Kalinina, N. O., Harrison, B. D., and Taliansky,
673 M. E. 2014. Coilin, the signature protein of Cajal bodies, differentially modulates the
674 interactions of plants with viruses in widely different taxa. Nucleus 5:85-94.

675 Scheets, K., Jordan, R., White, K.A., and Hernández, C., 2015. *Pelarspovirus*, a
676 proposed new genus in the family *Tombusviridae*. Arch. Virol. 160:2385-2393.

677 Scott, M. S., Boisvert, F. M., McDowall, M. D., Lamond, A. I., and Barton, G. J. 2010.
678 Characterization and prediction of protein nucleolar localization sequences. Nucleic
679 Acids Res. 38:7388-7399.

680 Sikorskaite, S., Rajamäki, M. L, Baniulis, D., Stanys, V., and Valkonen, J. P. 2013.
681 Protocol: Optimised methodology for isolation of nuclei from leaves of species in the
682 *Solanaceae* and *Rosaceae* families. Plant Methods 26:9:31.

683 Sit, T. L., and Lommel, S. A. 2015. *Tombusviridae*. In: eLS. J. Wiley and Sons, Ltd:
684 Chichester. DOI: 10.1002/9780470015902.a0000756.pub3.

685 Smith, H.M., Hicks, G.R., and Raikhel, N.V. 1997. Importin alpha from *Arabidopsis*
686 *thaliana* is a nuclear import receptor that recognizes three classes of import signals.
687 Plant Physiol. 114:411–417.

688 Taliansky, M. E., Brown, J. W. S., Rajamäki, M. L., Valkonen, J. P., and Kalinina, N.
689 O. 2010. Involvement of the plant nucleolus in virus and viroid infections: parallels
690 with animal pathosystems. Adv. Virus Res. 77:119-158.
691 Tao, T., Shi, H., Guan, Y., Huang, D., Chen, Y., Lane, D. P., Chen, J., and Peng, J.
692 2013. Def defines a conserved nucleolar pathway that leads p53 to proteasome-
693 independent degradation. Cell Res. 23:620-634.
694 Thole, V., Worland, B., Snape, J. W., and Vain, P. 2007. The pCLEAN dual binary
695 vector system for *Agrobacterium*-mediated plant transformation. Plant Physiol.
696 145:1211-1219.
697 Verwoerd, T. C., Dekker, M. M., and Hoekema, A. 1989. A small-scale procedure for
698 the rapid isolation of plant RNAs. Nucleic Acids Res. 17, 2362.
699 Wesley, S. V., Helliwell, C. A., Smith, N. A., Wang, M. B., Rouse, D.T., Liu, Q.,
700 Gooding, P. S., Singh, S. P., Abbott, D., Stoutjesdijk, P. A., Robinson,S. P., Gleave,
701 A. P., Green, A. G.. and Waterhouse, P. M. 2001. Construct design for efficient,
702 effective and high-throughput gene silencing in plants. Plant J. 27:581-590.
703 Zheng, L., Du, Z., Lin, C., Mao, Q., Wu, K., Wu, J., Wei, T., Wu, Z., and Xie, L. 2015.
704 Rice stripe tenuivirus p2 may recruit or manipulate nucleolar functions through an
705 interaction with fibrillarin to promote virus systemic movement. Mol. Plant Pathol.
706 16:921-930.
707

708 **FIGURE LEGENDS**

709

710 **Fig. 1**. Analysis of p37 localization through subcellular fractionation and Western blot
711 analysis. Aliquots of input extracts (IE), cytoplasmic fractions (Cit) and nuclear
712 fractions (Nuc), were subjected to SDS-PAGE followed by Western blot analysis using
713 either an anti-p37 (upper row), anti-UDP (middle row) or anti-H3 (lower row) antibody.
714 Extracts were prepared from *N. benthamiana* leaves transiently expressing a GFP-
715 tagged p37 (left panel) or an untagged p37 (central panel), or from systemic leaves
716 (right panel) of PLPV-infected *N. benthamiana*. Positions of p37, UDP and H3 are
717 indicated at the right.

718

719 **Fig. 2.** Subcellular distribution of p37-deletion derivatives with a C-terminal GFP tag.
720 (A) Schematic representation of PLPV p37 indicating the boundaries of the N-terminal
721 (Nt), middle (M) and C-terminal (Ct) domains. Amino acid (aa) sequence of the N-
722 terminal domain is detailed at the bottom; the aa stretch that has been determined here
723 as sufficient for nucleolar localization is within a square bracket, basic aa residues are in
724 red and aa residues that were previously shown to be essential for nucleolar localization
725 of a GFP-tagged p37 (Pérez-Cañamás & Hernández 2015) are underlined. B) Confocal
726 microscopy images showing the subcellular distribution of GFP-tagged p37 (p37:GFP)
727 and deletion derivatives ($p37_{1-77}$, $p37_{78-232}$, $p37_{233-338}$, $p37_{1-60}$, $p37_{1-45}$, $p37_{1-32}$, and $p37_{13-}$
728 $_{45}$:GFP) transiently expressed in *N. benthamiana* cells. The GFP-tagged proteins were
729 expressed along with an mRFP-tagged fibrillarin (Fib-mRFP, nucleolar marker).
730 Micrographs of the first column (starting from the left) show a general view of GFP-
731 derived fluorescence in epidermal cells expressing the distinct proteins. Micrographs of
732 the second and third columns show close-up view of GFP- and mRFP-derived

733 fluorescence, respectively, in individual cells and micrographs of the fourth column
734 show merged images of GFP and mRFP signals in such individual cells. The nucleus
735 (N) is marked by an arrow in fourth column panels. The *inset* scale bar corresponds to
736 10 μm in all panels.
737
738 **Fig. 3.** Analysis of potential interaction(s) between p37 and representative members of
739 importin alpha family through BiFC and co-immunoprecipitation assays. A)
740 Phylogenetic tree of the fourteen members of importin alpha family encoded by *N.*
741 *benthamiana*. Alignments were made using ClustalW and the trees was generated by
742 neighbor-joining (N-J) method using complete deletion treatments with MEGA7.
743 Numbers at branches show the percentage bootstrap support (if >50 %) for 1,000
744 replicates. The scales indicate JTT amino acid distances. *Phytophthora infestans*
745 importin alpha was used as outgroup. Numbers represent accessions from the Sol
746 genomics database and GenBank accession numbers. The layout of the tree was
747 essentially identical to that obtained by Lukhovitskaya et al. (2016) with sequences
748 retrieved from Sol Genomics Network though, in the present case, an updated version of
749 the database has been used for phylogenetic analysis. Importins alpha employed in this
750 study as representatives of clade I, II and III, respectively, are denoted in red, green and
751 blue. B) p37 and importin alpha molecules were tagged at their N-terminus with sYFP
752 halves (sYFPN and sYFPC) and transiently co-expressed in *N. benthamiana* leaves to
753 study protein-protein interactions through a BiFC assay. An mRFP-tagged fibrillarin
754 (Fib-mRFP), employed as nucleolar marker, was also co-expressed. Confocal laser-
755 scanning microscopy was used for the observation of fluorescence at 3 d.p.if. For each
756 protein combination, micrographs at the left show a general view of YFP-derived
757 fluorescence in epidermal cells (*inset* scale bar, 10 μm). Micrographs of the second and

758 third columns show close-up view of YFP- and mRFP-derived fluorescence,
759 respectively, in individual cells and micrographs of the fourth column show merged
760 images of YFP and mRFP signals in such individual cells (*inset* scale bar, 10 μm). The
761 nucleus (N) is marked by an arrow in fourth column panels. A negative control
762 combination (sYFPN:p37 plus sYFPC) is displayed in row F. Equivalent images were
763 obtained with the reverse combinations (YFPC:p37 co-expressed with sYFPN-tagged
764 importins alpha) (data not shown). C) Western blot analysis of protein preparations.
765 Importin alpha molecules of clade III and subclade Ia were fused at their C-terminus
766 with an His-tag and expressed in *N. benthamiana* leaves either alone or in combination
767 with p37. Input protein extracts (left panel) or immunoprecipitates (IP) (right panel)
768 obtained with anti-His antibody were subjected to Western blot (Wb) analysis using
769 either an anti-His antibody (for detection of importins alpha; upper blots) or an anti-p37
770 antisera (for detection of p37; lower blots).
771
772 **Fig. 4**. Effect of silencing of importins alpha on the nucleolar localization of p37. *N.*
773 *benthamiana* leaves were agroinfiltrated with RNAi constructs to direct silencing of
774 importins alpha included in clades/subclades II, III, Ia, Ib and/or Ic. Leaves
775 agroinfiltrated with an empty RNAi vector were used as controls. A) Semiquantitative
776 RT-PCR to corroborate the reduction of importin alpha transcript levels in leaves
777 agroinfiltrated with a mixture of RNAi constructs designed to silence importins alpha
778 belonging to all clades/subclades (lanes "Imp α") in comparison to leaves
779 agroinfiltrated with an empty RNAi vector (lanes "Empty). B) Semiquantitative RT-
780 PCR to assess transcript levels of importins alpha of the different clade/subclades in
781 leaves agroinfiltrated with the RNAi construct designed to silence importins alpha
782 belonging to subclade Ia (lanes "Imp α Ia") in comparison to leaves agroinfiltrated with

783 an empty RNAi vector (lanes "Empty"). In both panels, A and B, Samples for analysis
784 were collected at 5 d.p.if. and the transcript accumulation levels of importins alpha of
785 the distinct clades/subclades were evaluated using appropriate pairs of primers. C) At
786 the top, representative confocal microscopy images showing the intracellular
787 distribution of transiently GFP-tagged p37 in plant cells in which expression of all
788 importins alpha was either impaired (RNAi-Imp α) or not impaired (RNAi-Empty).
789 Fluorescence was visualized 72 h after agroinfiltration of the GFP-tagged p37 construct.
790 Images corresponding to plant cells depleted for importins alpha of the different
791 clades/subclades or depleted simultaneously for all of them were taken to estimate the
792 percentage of cells in which p37 showed a nucleolar localization. The average number
793 of cells included for counting was of 60 and the calculated percentages are shown in the
794 table at the bottom.
795
796 **Fig. 5.** Importin alpha depletion negatively affects *in vivo* PLPV accumulation. *N.*
797 *benthamiana* leaves were agroinfiltrated with an RNAi empty construct (mock control)
798 or with mixture of RNAi constructs to direct silencing of all importins alpha. Five days
799 after infiltration (d.p.if), the same leaves were agroinoculated with a full-length cDNA
800 clone of PLPV. Leaf samples were harvested at different days after virus inoculation
801 (d.p.i.). A) Northern blot analysis for PLPV detection in samples collected at 1, 2, 3,
802 and 7 d.p.i. from either mock controls (lanes a-d) or importin alpha-silenced leaves
803 (lanes e-h). The positions of the genomic (g) and subgenomic (sg) RNAs of PLPV are
804 indicated at the right. Note that the virus was barely detectable at 1 d.p.i. in either case
805 because its low accumulation levels. Ethidium bromide staining of rRNAs is shown
806 below the blots as loading control. Discontinuous lines indicate lanes that were not
807 contiguous in the original gel. B) RT-qPCR to estimate relative PLPV accumulation

808 (left panel) and relative levels of importin α1 transcripts (right panel) at 3 and 7 d.p.i. In

809 B and C, bars depict standard deviations from three independent biological replicates.

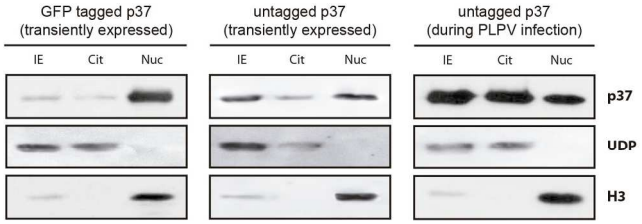

Fig. 1. Analysis of p37 localization through subcellular fractionation and Western blot analysis. Aliquots of input extracts (IE), cytoplasmic fractions (Cit) and nuclear fractions (Nuc), were subjected to SDS-PAGE followed by Western blot analysis using either an anti-p37 (upper row), anti-UDP (middle row) or anti-H3 (lower row) antibody. Extracts were prepared from N. benthamiana leaves transiently expressing a GFP-tagged p37 (left panel) or an untagged p37 (central panel), or from systemic leaves (right panel) of PLPV-infected N. benthamiana. Positions of p37, UDP and H3 are indicated at the right.

131x223mm (300 x 300 DPI)

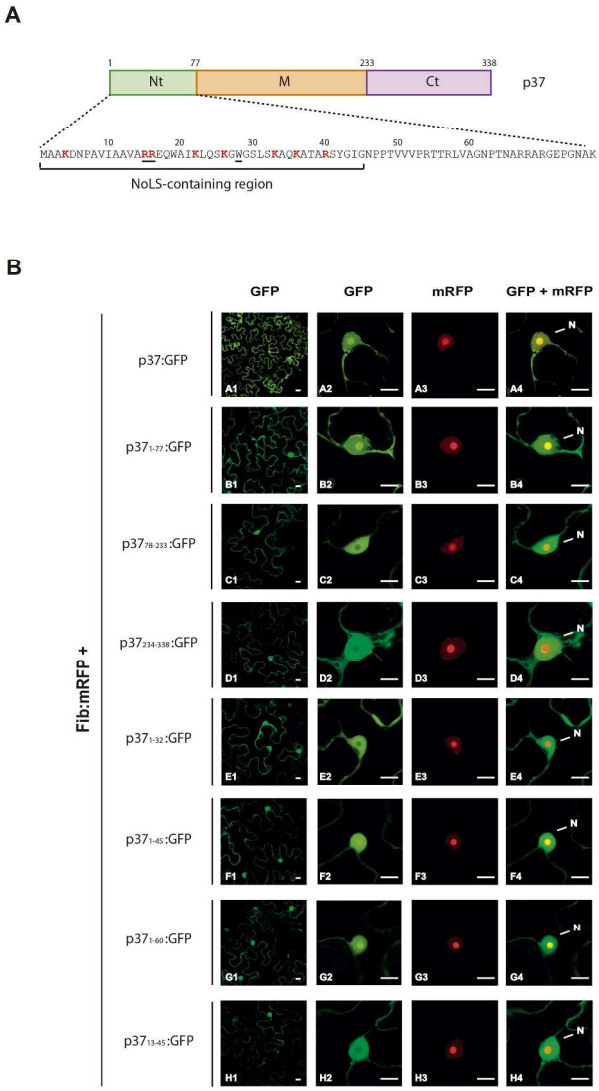

Fig. 2. Subcellular distribution of p37-deletion derivatives with a C-terminal GFP tag. (A) Schematic representation of PLPV p37 indicating the boundaries of the N-terminal (Nt), middle (M) and C-terminal (Ct) domains. Amino acid (aa) sequence of the N-terminal domain is detailed at the bottom; the aa stretch that has been determined here as sufficient for nucleolar localization is within a square bracket, basic aa residues are in red and aa residues that were previously shown to be essential for nucleolar localization of a GFP-tagged p37 (Pérez-Cañamás & Hernández 2015) are underlined. B) Confocal microscopy images showing the subcellular distribution of GFP-tagged p37 (p37:GFP) and deletion derivatives (p371-77, p3778-232, p37233-338, p371-60, p371-45, p371-32, and p3713-45:GFP) transiently expressed in N. benthamiana cells. The GFP-tagged proteins were expressed along with an mRFP-tagged fibrillarin (Fib-mRFP, nucleolar marker). Micrographs of the first column (starting from the left) show a general view of GFP-derived fluorescence in epidermal cells expressing the distinct proteins. Micrographs of the second and third columns show close-up view of GFP- and mRFP-derived fluorescence, respectively, in individual cells and micrographs of the fourth column show merged images of GFP and mRFP signals in such individual cells. The nucleus (N)

is marked by an arrow in fourth column panels. The inset scale bar corresponds to 10 μm in all panels.

175x266mm (300 x 300 DPI)

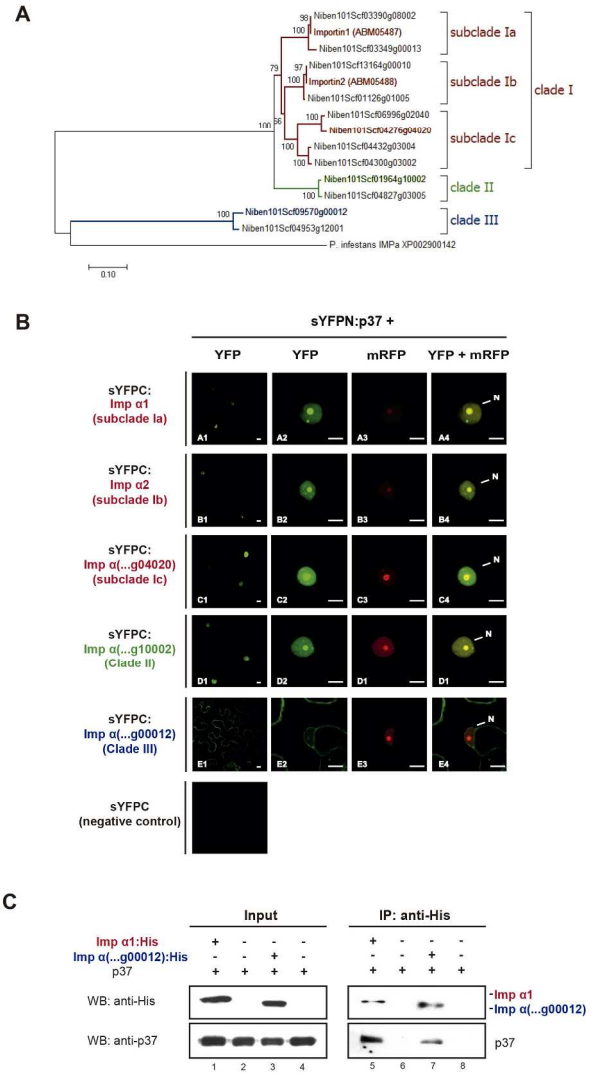

Fig. 3. Analysis of potential interaction(s) between p37 and representative members of importin alpha family through BiFC and co-immunoprecipitation assays. A) Phylogenetic tree of the fourteen members of importin alpha family encoded by N. benthamiana. Alignments were made using ClustalW and the trees was generated by neighbor-joining (N-J) method using complete deletion treatments with MEGA7. Numbers at branches show the percentage bootstrap support (if >50 %) for 1,000 replicates. The scales indicate JTT amino acid distances. Phytophthora infestans importin alpha was used as outgroup. Numbers represent accessions from the Sol genomics database and GenBank accession numbers. The layout of the tree was essentially identical to that obtained by Lukhovitskaya et al. (2016) with sequences retrieved from Sol Genomics Network though, in the present case, an updated version of the database has been used for phylogenetic analysis. Importins alpha employed in this study as representatives of clade I, II and III, respectively, are denoted in red, green and blue. B) p37 and importin alpha molecules were tagged at their N-terminus with sYFP halves (sYFPN and sYFPC) and transiently co-expressed in N. benthamiana leaves to study protein-protein interactions through a BiFC assay. An mRFP-tagged fibrillarin (Fib-mRFP), employed as

nucleolar marker, was also co-expressed. Confocal laser-scanning microscopy was used for the observation of fluorescence at 3 d.p.if. For each protein combination, micrographs at the left show a general view of YFP-derived fluorescence in epidermal cells (inset scale bar, 10 μm). Micrographs of the second and third columns show close-up view of YFP- and mRFP-derived fluorescence, respectively, in individual cells and micrographs of the fourth column show merged images of YFP and mRFP signals in such individual cells (inset scale bar, 10 μm). The nucleus (N) is marked by an arrow in fourth column panels. A negative control combination (sYFPN:p37 plus sYFPC) is displayed in row F. Equivalent images were obtained with the reverse combinations (YFPC:p37 co-expressed with sYFPN-tagged importins alpha) (data not shown). C) Western blot analysis of protein preparations. Importin alpha molecules of clade III and subclade Ia were fused at their C-terminus with an His-tag and expressed in N. benthamiana leaves either alone or in combination with p37. Input protein extracts (left panel) or immunoprecipitates (IP, right panel) obtained with anti-His antibody were subjected to Western blot (Wb) analysis using either an anti-His antibody (for detection of importins alpha; upper blots) or an anti-p37 antisera (for detection of p37; lower blots).

166x278mm (300 x 300 DPI)

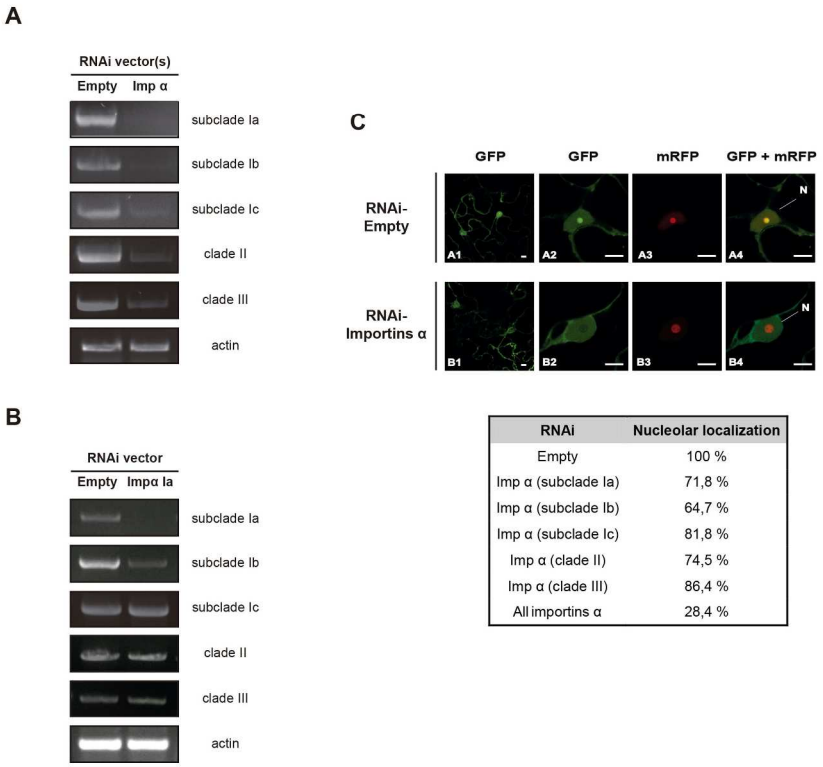

RNAi	Nucleolar localization
Empty	100 %
Imp α (subclade Ia)	71,8 %
Imp α (subclade Ib)	64,7 %
Imp α (subclade Ic)	81,8 %
Imp α (clade II)	74,5 %
Imp α (clade III)	86,4 %
All importins α	28,4 %

Fig. 4. Effect of silencing of importins alpha on the nucleolar localization of p37. N. benthamiana leaves were agroinfiltrated with RNAi constructs to direct silencing of importins alpha included in clades/subclades II, III, Ia, Ib and/or Ic. Leaves agroinfiltrated with an empty RNAi vector were used as controls. A) Semiquantitative RT-PCR to corroborate the reduction of importin alpha transcript levels in leaves agroinfiltrated with a mixture of RNAi constructs designed to silence importins alpha belonging to all clades/subclades (lanes "Imp α") in comparison to leaves agroinfiltrated with an empty RNAi vector (lanes "Empty). B) Semiquantitative RT-PCR to assess transcript levels of importins alpha of the different clade/subclades in leaves agroinfiltrated with the RNAi construct designed to silence importins alpha belonging to subclade Ia (lanes "Imp α Ia") in comparison to leaves agroinfiltrated with an empty RNAi vector (lanes "Empty"). In both panels, A and B, samples for analysis were collected at 5 d.p.if. and the transcript accumulation levels of importins alpha of the distinct clades/subclades were evaluated using appropriate pairs of primers. C) At the top, representative confocal microscopy images showing the intracellular distribution of transiently GFP-tagged p37 in plant cells in which expression of all importins

alpha was either impaired (RNAi-Imp α) or not impaired (RNAi-Empty). Fluorescence was visualized 72 h after agroinfiltration of the GFP-tagged p37 construct. Images corresponding to plant cells depleted for importins alpha of the different clades/subclades or depleted simultaneously for all of them were taken to estimate the percentage of cells in which p37 showed a nucleolar localization. The average number of cells included for counting was of 60 and the calculated percentages are shown in the table at the bottom.

184x256mm (300 x 300 DPI)

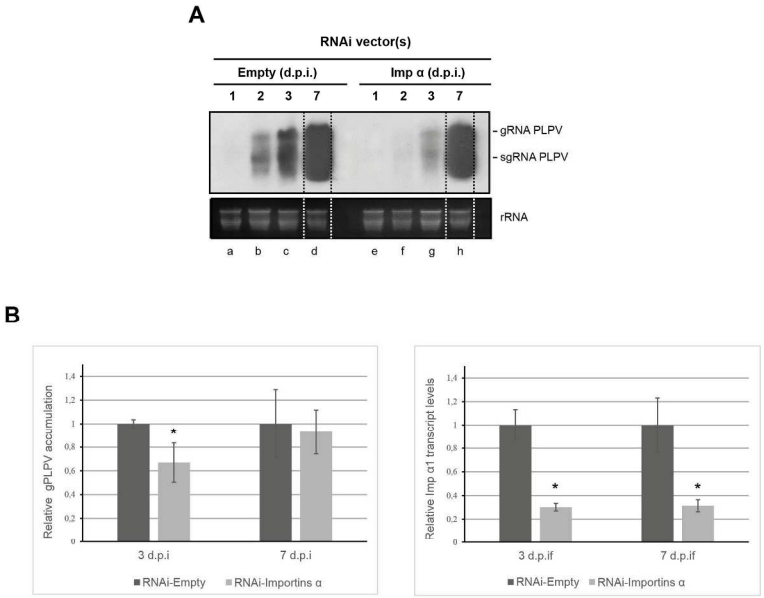

Fig. 5. Importin alpha depletion negatively affects in vivo PLPV accumulation. N. benthamiana leaves were agroinfiltrated with an RNAi empty construct (mock control) or with mixture of RNAi constructs to direct silencing of all importins alpha. Five days after infiltration (d.p.if), the same leaves were agroinoculated with a full-length cDNA clone of PLPV. Leaf samples were harvested at different days after virus inoculation (d.p.i.). A) Northern blot analysis for PLPV detection in samples collected at 1, 2, 3, and 7 d.p.i. from either mock controls (lanes a-d) or importin alpha-silenced leaves (lanes e-h). The positions of the genomic (g) and subgenomic (sg) RNAs of PLPV are indicated at the right. Note that the virus was barely detectable at 1 d.p.i. in either case because its low accumulation levels. Ethidium bromide staining of rRNAs is shown below the blots as loading control. Discontinuous lines indicate lanes that were not contiguous in the original gel. B) RT-qPCR to estimate relative PLPV accumulation (left panel) and relative levels of importin α1 transcripts (right panel) at 3 and 7 d.p.i. In B and C, bars depict standard deviations from three independent biological replicates.

193x258mm (300 x 300 DPI)

Supplementary Table S1. List of primers used in this work

p37 deletion constructs

Primer	Position[a]	Sequence[b]		Construct or gene
CH362	2621-2647 (S)	5´- GTGGATCCATGGCGGCCAAGGATAATC -3´	(*Bam*HI)	35S:p37$_{1-77}$:GFP
CH530	2832-2851 (AS)	5´- GTCCATGGCTTTGGCATTACCCGGCTCTC -3´	(*Nco*I)	
CH531	2852-2872 (S)	5´- CCGGATCCATGGGCACCACCATAACCAAG -3´	(*Bam*HI)	35S:p37$_{78-233}$:GFP
CH532	3301-3319 (AS)	5´- GTCCATGGCGGTTGGTTCAGAAAACACG -3´	(*Nco*I)	
CH533	3320-3336 (S)	5´- CCGGATCCatgTTCTGCACCCACCACTC -3´	(*Bam*HI)	35S:p37$_{234-338}$:GFP
CH385	3615-3634 (AS)	5´- CCGGATCCCAGCTTGTTGATGTAAGCTC -3´	(*Bam*HI)	
CH362	2621-2647 (S)	5´- GTGGATCCATGGCGGCCAAGGATAATC -3´	(*Bam*HI)	35S:p37$_{1-32}$:GFP
CH691	2698-2716 (AS)	5´- CCGGATCCGGACAAAGAGCCCCAACC -3´	(*Bam*HI)	
CH362	2621-2647 (S)	5´- GTGGATCCATGGCGGCCAAGGATAATC -3´	(*Bam*HI)	35S:p37$_{1-45}$:GFP
CH702	2737-2755 (AS)	5´- CCGGATCCCCCGATCCCGTACGAGCG -3´	(*Bam*HI)	
CH362	2621-2647 (S)	5´- GTGGATCCATGGCGGCCAAGGATAATC -3´	(*Bam*HI)	35S:p37$_{1-60}$:GFP
CH703	2782-2800 (AS)	5´- GAGGATCCTGCCACCAGCCGGGTAGTG -3´	(*Bam*HI)	
CH710	2657-2676 (S)	5´- GTGGATCCATGGCAAGACGGGAACAGTG -3´	(*Bam*HI)	35S:p37$_{13-45}$:GFP
CH702	2737-2755 (AS)	5´- CCGGATCCCCCGATCCCGTACGAGCG -3´	(*Bam*HI)	

BiFC constructs

CH640	1-21 (S)	5´- GTGGATCCATGTCGCTGAGGCCGAATTCG -3´	(*Bam*HI)	sYFPN:Imp α1
CH641	1579-1599 (AS)	5´- GTAAGCTTGGTACCTCATGAACTGAAGTTGAATC -3´	(*Hind*III *Bam*HI)	sYFPC:Imp α1
CH643	1-21 (S)	5´- CAGGATCCATGTCTCTGAGACCAAGTGCT -3´	(*Bam*HI)	sYFPN:Imp α2
CH644	1579-1599 (AS)	5´- GTAAGCTTGAATTCCCGGGTCAACCAAACTTGAATCCAC-3´	(*Hind*III *Eco*RI *Sma*I)	sYFPC:Imp α2
CH658	1-23 (S)	5´- CAGGATCCATGTCGCTGAGACCTAGTGCGAG -3´	(*Bam*HI)	sYFPN:Imp α(…g04020)
CH659	1623-1644 (AS)	5´- CCGGTACCTCAGTTAAAGTTGAATCCACC -3´	(*Kpn*I)	sYFPC:Imp α(…g04020)
CH704	1-23 (S)	5´- CAGGATCCATGTCTCTTCGACCCGGCACTCG -3´	(*Bam*HI)	sYFPN:Imp α(…g10002)
CH705	1575-1596 (AS)	5´- CCGGTACCTTACCCAAACTTGAATCCACC -3´	(*Kpn*I)	sYFPC:Imp α(…g10002)
CH706	1-25 (S)	5´- CAGGATCCATGGCAGATGAAGTGGGCAATGCTG -3´	(*Bam*HI)	sYFPN:Imp α(…g00012)
CH707	1453-1473 (AS)	5´- CCGGTACCTATTCATCAAGTCCATATTC -3´	(*Kpn*I)	sYFPC:Imp α(…g00012)

Co-Immunoprecipitation

CH640	1-21 (S)	5´- GTGGATCCATGTCGCTGAGGCCGAATTCG -3´	(*Bam*HI)	35S:Imp α1:His
CH782	1579-1599 (AS)	5´- TACCCGGGTCAGTGGTGATGGTGATGATGTGCTGC TGAACTGAAGTTGAATC -3´	(*Sma*I)	
CH706	1-25 (S)	5´- CAGGATCCATGGCAGATGAAGTGGGCAATGCTG -3´	(*Bam*HI)	35S:Imp α(…g00012):His
CH783	1453-1473 (AS)	5´- GTCCCGGGTCAGTGGTGATGGTGATGATGTGCTGC TTCATCAAGTCCATATTC -3´	(*Sma*I)	

RNAi constructs

CH642	1256-1276 (S)	5´- CAGGATCCTCGAGTGTGCGATCTTCTGGTTTGT -3´	(*Bam*HI *Xho*I)	pClean- Imp α(clade Ia)
CH641	1579-1599 (AS)	5´- GTAAGCTTGGTACCTCATGAACTGAAGTTGAATC -3´	(*Hind*III *Bam*HI)	
CH645	1256-1276 (S)	5´- CTGGATCCTCGAGTATGTGATTTGCTTGTGTGC -3´	(*Bam*HI *Xho*I)	pClean- Imp α(clade Ib)
CH644	1570-1590 (AS)	5´- GTAAGCTTGAATTCCCGGGTCAACCAAACTTGAATCCAC-3´	(*Hind*III-*Eco*RI-*Sma*I)	
CH652	521-540 (S)	5´- CATCTAGACTCGAGTCCGAGAGCAGGCTGTGTG -3´	(*Xba*I-*Xho*I)	pClean-Imp α(clade Ic)
CH653	838-857 (AS)	5´- CAGGATCCGAATTCATACTCCAGAATCAATAAC -3´	(*Bam*HI-*Eco*RI)	
CH654	388-408 (S)	5´- GATCTAGACTCGAGCCTCAGCTTCAATTTGAAGC -3´	(*Xba*I-*Xho*I)	pClean-Imp α(clade II)
CH655	817-836 (AS)	5´- CAGGATCCGAATTCGCCTGAATCTTATCATTTGG -3´	(*Bam*HI-*Eco*RI)	
CH656	378-397 (S)	5´- CGTCTAGACTCGAGCTCTCCAGATGAACAGTTGC -3´	(*Xba*I-*Xho*I)	pClean-Imp α(clade III)
CH657	781-800 (AS)	5´- CAGGATCCGAATTCACAACAACCCATGCTACTTC -3´	(*Bam*HI-*Eco*RI)	

Semiquantitative RT-PCR

CH640	1-21 (S)	5´- GTGGATCCATGTCGCTGAGGCCGAATTCG -3´	(*Bam*HI)	Imp α1
CH641	1579-1599 (AS)	5´- GTAAGCTTGGTACCTCATGAACTGAAGTTGAATC -3´	(*Hind*III *Bam*HI)	
CH643	1-21 (S)	5´- CAGGATCCATGTCTCTGAGACCAAGTGCT -3´	(*Bam*HI)	Imp α2
CH644	1579-1599 (AS)	5´- GTAAGCTTGAATTCCCGGGTCAACCAAACTTGAATCCAC-3´	(*Hind*III *Eco*RI *Sma*I)	
CH658	1-23 (S)	5´- CAGGATCCATGTCGCTGAGACCTAGTGCGAG -3´	(*Bam*HI)	Imp α(…g04020)
CH661	1120-1146 (AS)	5´- CACTGCAGCAAGAGTAGTGTACTTTG -3’	(*Kpn*I)	
CH704	1-23 (S)	5´- CAGGATCCATGTCTCTTCGACCCGGCACTCG -3´	(*Bam*HI)	Imp α(…g10002)
CH655	817-836 (AS)	5´- CAGGATCCGAATTCGCCTGAATCTTATCATTTGG -3´	(*Bam*HI-*Eco*RI)	
CH706	1-25 (S)	5´- CAGGATCCATGGCAGATGAAGTGGGCAATGCTG -3´	(*Bam*HI)	Imp α(…g00012)
CH657	781-800 (AS)	5´- CAGGATCCGAATTCACAACAACCCATGCTACTTC -3´	(*Bam*HI-*Eco*RI)	

Quantitative RT-PCR

CH718	85-104 (S)	5´- CGCTCCTCGGTCCTAACTTG -3´	-	p27 PLPV
CH719	166-185 (AS)	5´- ATTTTGGCCAACCCATGGA -3´	-	
CH436		5´- ACTTGGTGCCCTTTGTATGC -3´	-	PP2A
CH437		5´- TGGACCAAATTCTTCTGCAA -3´	-	
CH750	1110-1129 (S)	5´- TGGCATTATTGCCCCTCTTG -3´	-	Imp α1
CH751	1190-1209 (AS)	5´- ATTTCCACCGGACGTAGCAT -3´	-	

[a] Positions of the PLPV genome or Importins genes covered by the primers. (S) and (AS): sense and antisense.

[b] Restriction sites introduced for cloning purposes are underlined and lowercase indicate nucleotide substitutions to PLPV wt sequence.